Ultrasonication of spray- and freeze-dried cellulose nanocrystals in water

Quentin BEUGUEL, Jason R. TAVARES, Pierre J. CARREAU, Marie-Claude HEUZEY

Department of Chemical Engineering, CREPEC – Research Center on High Performance Polymer and Composite Systems, Polytechnique Montreal, Montreal, QC, H3T 1J4, Canada.

Corresponding author: Marie-Claude Heuzey (E-mail: marie-claude.heuzey@polymtl.ca, +1 (514) 340-4711 ext. 5930

Abstract

The structural and rheological properties of aqueous suspensions of spray-dried cellulose nanocrystals (CNCs) were investigated and compared to those of freeze-dried. The cellulose nanocrystals were obtained from sulfuric acid hydrolysis of wood pulp. Ultrasonication was used to disperse cellulose nanocrystals in Milli-Q water and the power applied during ultrasonication was shown to be the controlling parameter for their dispersion, more than total energy. Dynamic light scattering measurements showed a decrease of the average hydrodynamic diameter down to the same limiting value, *i.e.* ~ 75 nm, for both spray and freeze-dried cellulose nanocrystals. Since the same maximum dispersion state was reached for both CNC types, it indicated that the spray drying process did not limit dispersion, provided that sufficient ultrasonication was provided. Moreover, no desulfation occurred during ultrasonication at ambient temperature. Strong ultrasonication also caused a decrease of intrinsic viscosity, along with an increase in maximum packing concentration. These properties were correlated to agglomerates break-up, which released both ions and water in suspension. The ionic strength increase may lead to a thinner electrostatic double layer surrounding the cellulose nanocrystals, reducing their apparent concentration.

Keywords: cellulose nanocrystals (CNCs); spray drying; ultrasonication; aqueous suspension; structure; rheology

1. Introduction

Since the early 2000s, biodegradable and biosourced cellulose nanocrystals (CNCs) have been widely studied for their high stiffness and large aspect ratio, in order to improve the mechanical properties of thermoplastics [1–3]. The CNC source and extraction method influence their final physicochemical properties [4–8]. Surface ionic groups and high polarity favor CNC dispersion at the nanoscale in water [9] or in polar thermoplastics prepared by solution mixing [6,10,11]. However, only a few approaches for non-polar thermoplastic nanocomposite elaboration by melt mixing have been investigated [12–14]. This is in large part because of dispersion issues: spray or freeze-drying processes [9] are used to prepare CNCs [15], but these cause strong particle agglomeration [16,17]. Thus CNCs are difficult to redisperse for chemical modification [18,19] or to obtain nanocomposites. Spray- and freeze-drying processes lead to various CNC powder properties [20], especially in terms of bulk density and porosity [21,22], suggesting different possible dispersion states in a solvent [9]. Agglomerate break-up is difficult to achieve, especially for the smallest ones [21], but can be achieved through ultrasonication. This process, based on cavitation phenomena [23], was demonstrated to be efficient to redisperse CNCs in aqueous suspensions [24–26]. An ultrasonication time of a few hundreds of seconds [27–29] or an energy of a few thousand joules per gram of CNCs [9,30] enables the break-up of agglomerates. Moreover, ultrasounds could also cause disruption of the electrostatic double layer surrounding the CNC particles [24]. However, the influence of these parameters has scarcely been investigated. Rheological properties may provide an interesting avenue, as these have been widely studied for electrostabilized colloidal suspensions, taking into account both the particle size and their electrostatic double layer thickness [31,32]. The interest of rheology as a tool to characterize CNC aqueous suspensions was demonstrated recently [33], with three concentration-dependent behaviors identified: i) isotropic at low concentrations, ii) lyotropic liquid crystal due to the chiral nematic structure [34,35] of CNCs, at intermediate concentrations and, finally, iii) gel, at high concentrations [30,36]. The threshold concentrations can be correlated with the nanoparticle aspect ratio [33]. The surface groups [37] and their charge density [38,39] also affect the rheological behavior of CNC suspensions. For example, Shafiei-Sabet *et al.* [38] showed lower viscosity values for aqueous suspensions containing CNCs with a higher content of ionic groups on their surface. On the other hand, the addition of salts can modify the electrostatic double layer and disturb the electrostatic repulsion, which first reduces the viscosity and then leads to gel formation by flocculation [40–42]. Finally, high

temperatures [43] or ultrasonication energy [30] may change the rheological behavior of CNC suspensions, by increasing the size of chiral nematic domains. Models based on the Einstein equation [44] for hard sphere suspensions have been proposed to explain the rheological behavior of CNC suspensions, using intrinsic viscosity data. For example, the Huggins [45] and Fedors [46] models, classically used for polymers in dilute and semi-dilute regimes, have been adapted to fit the relative viscosity variations of CNC suspensions as a function of concentration [36,40,47–49]. However, no consensus on the mechanisms and parameters controlling the rheological properties of these suspensions has been reached.

The aim of this study is to improve our knowledge on the behavior of CNCs in aqueous suspensions, accounting for their industrial preparation method (spray drying), without additional modification. Moreover, special attention is paid to the ultrasonication method used to redisperse CNCs, both in terms of energy and power.

2. Materials and methods

The CNCs were obtained from sulfuric acid hydrolysis of wood pulp [7], inducing sulfate half ester groups O-SO_3H on the CNC surface [50], easily deprotonated due to their low pKa close to 0. CNCs used in this study were supplied, in dry form after neutralization with sodium hydroxide (NaOH) and spray or freeze drying processes [9], by CelluForce (Montreal, Canada) and FPInnovations (Pointe Claire, Canada), respectively. The density of CNCs was taken equal to 1,540 $kg.m^{-3}$.

CNC suspensions at ϕ = 5 wt% were ultrasonicated using a Sonics & Materials VCX500 probe, operating at 20 kHz, with power P of 10, 50 and 90 W and energy E ranging from 2,500 to 10,000 J/g_{CNC}. The volume in the glass container used was ~ 40 cm^3 (2.9 cm height by 2.1 cm radius); it was placed in an ice bath while ultrasonication was applied in various pulse cycles: 10 s ON / 1 s OFF for P = 10 W, and of 1 s ON / 1 s OFF for P = 50 and 90 W, to avoid overheating. Then, the CNC suspensions were diluted with Milli-Q water (at 18.2 MΩ.cm) to obtain a weight fraction range ϕ from 0 to 5 wt%.

The electric conductivity σ of spray-dried CNC suspensions before and after an ultrasonication at P = 50 W and E = 10,000 J/g_{CNC} was measured at room temperature using a conductimeter Inolab pH/Ion/Cond 750 (WTW). The average value of σ was calculated from 5 measurements and the data are accurate to ± 20 µS/cm.

Quantitative elemental analysis was performed with a Tabletop Hitachi TM3030+ scanning electron microscope (SEM), operating at 15kV and equipped with X-Ray spectroscopy (EDX). Such analyses were conducted on CNC powders or flat films obtained after a slow drying of the suspension under vacuum. The number of sulfate groups attached on the CNC surface was determined from measurements before and after suspension dialysis in Milli-Q water. 25 mL of the CNC suspension (ϕ = 1 wt%) was dialysed for 2 h through a Spectra/Por 2 12-14 kDa Standard Regenerated Cellulose porous membrane (Spectrumlabs) using 2.5 L of water. This step was repeated three times for each sample. For all samples, the average atomic ratio of sulfur to carbon (S/C) was obtained from 10 measurements of X-rays emitted (acquired for 60 s, each), on different areas.

Nanometer-scale observations were performed using a Jeol JEM 2100F transmission electronic microscope (TEM) bright field imaging, under focus to maximize contrast, operating at 200 kV. The suspensions were diluted to ϕ = 0.001 wt% and dried, on copper TEM grids (Electron Microscopy Sciences) with a thin film (5 – 6 nm) of pure carbon deposited on one side (CF200-Cu), for 30 min. The average length L_0, diameter d_0 and aspect ratio p_0 of individual CNCs were measured on 100 particles at least for each sample. The average values are accurate to ± 10%.

Micrometer-scale observations were performed in order to show any isotropic or anisotropic structures in the CNC suspensions (ϕ ranging from 3 to 7 wt%). These were conducted with a Zeiss Axio Scope A1 optical microscope, equipped with a QImaging QICAM-12-bit camera and cross polarizer.

Zeta potential measurements, related to the particle electrophoretic mobility through the Smoluchowski equation [51], were performed on 0.2 wt% CNC suspensions (prepared in different conditions) at 25 °C, using a Malvern Zetasizer Nano-ZS (DTS1070 cell). These measurements characterized the particle charge density, quasi-independently of their size

[52]. The average value of 5 successive measurements (10 runs of 15 s each) was determined. The same instrument was used to measure the particle size by dynamic light scattering (DLS). Tests were carried out in backscattering mode at an angle of 173°. The particle number and volume size distributions were inferred from the intensity, considering refractive and adsorption indices of 1.59 and 0.01, respectively. Each curve was an average measured for three different fractions (ϕ = 0.05, 0.1 and 0.2 wt%), all of them obtained from 5 successive measurements of 10 runs of 15 s each. Volume average D_v and number average D_n diameters were calculated to determine the average polydispersity index D_v/D_n. The *Z*-average, representing the intensity-weighted mean hydrodynamic diameter, was also reported. These values are accurate to ± 10 %.

Rheological tests were carried out using a controlled stress rheometer, MCR502 (Anton Paar), equipped with a double-wall Couette flow geometry. Time sweep measurements in the linear domain showed that the viscoelastic properties of the CNC suspension (ϕ = 3 wt%) were stable for 10 h. In addition, for all suspensions, frequency sweep (ω ranging from 100 rad.s^{-1} to 10^{-2} rad.s^{-1}) at a strain within the linear viscoelastic regime, and shear rate ($\dot{\gamma}$ ranging from 0.5 to 500 s^{-1}) tests were performed. These tests were conducted at T = 25°C, within a maximum time frame of 10 h after ultrasonication. All rheological tests were performed after a pre-shear of 100 s at 10 s^{-1} and a rest time of 180 s, to homogenize the suspensions. Rheological tests were reproducible to ± 10%.

3. Results

3.1 Ionic charge properties

The conductivity σ of a 5 wt% spray-dried CNC suspension, without salt addition (pH close to 6.8), before and after a strong ultrasonication (P = 50 W and E = 10,000 J/g$_{CNC}$) increases from ~ 400 to 540 µS.cm^{-1} attributed to the higher number of ions available in water, as observed by Beck *et al.* [24]. According to Sposito's [53] work on soil solutions, the empirical relation of Marion-Babcock [54] between the ionic strength (in mol.m^{-3}) and the electrical conductivity (in dS.m^{-1}) is accurate for ionic strengths up to about 300 mol.m^{-3}:

$$\log I = 1.159 + 1.009 \log \sigma \qquad (1)$$

Using Eq.1, the ionic strength I increases from 5.7 to 7.7 mol.m^{-3}, before and after a strong ultrasonication. Then, the Debye-Hückel length K^{-1}, characterizing the electrostatic double layer thickness can be calculated [55]:

$$K^{-1} = \sqrt{\frac{\varepsilon_r \varepsilon_0 k_B T}{2e^2 N_A I}} \quad (2)$$

where ε_r, ε_r, k_B, T, e and N_A are the relative and vacuum permittivity, the Boltzmann constant, the temperature, the net charge of an electron and the Avogadro's number, respectively. K^{-1} is ranging from ~ 4.1 to 3.5 nm for non- and strong ultrasonicated CNC suspensions, close to the value estimated by titration to neutralize never-dried CNC suspension (pH close to 3) with NaOH solution up to a pH = 7. Indeed, the addition of ~ 4 mL of NaOH at 100 mol.m^{-3} was necessary to neutralize 40 mL of the 5 wt% never-dried CNC suspension. The resulting ionic strength related to the ion concentration was calculated from Eq. (3) [49]:

$$I = \frac{1}{2}\sum_i C_i z_i^2 \quad (3)$$

where C_i is the molar concentration of solvated ions and z_i their valence, resulting in I = 10 mol.m^{-3} and Debye-Hückel length K^{-1} of 3.1 nm (Eq. 2), in agreement with the above estimates.

Figure 1 presents the S/C atomic ratio measured by EDX for spray-dried and freeze-dried CNC suspensions, before and after dialysis, and after ultrasonication at P = 50 W and E = 10,000 J/g_{CNC}.

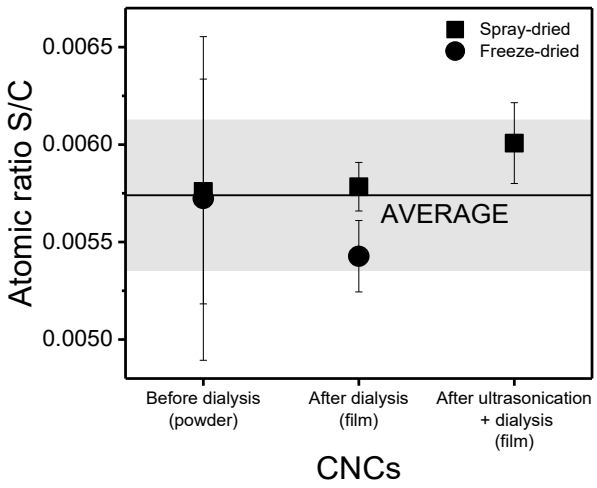

Figure 1: Atomic ratio S/C for CNC suspensions. The grey area represents the average standard deviation.

The standard deviation for the S/C ratio measured for the CNC powders before dialysis is higher than for CNC flat films after dialysis and could be due to surface topography. For all samples, the S/C atomic ratio is close to 0.0057, corresponding to 3.4 O-SO_3H groups per 100 anhydroglucose units and a substitution degree *SD* ~ 1.15%, considering three hydroxyl groups (OH) per glucose unit, in the same order of magnitude as the value reported by Sojoudiasli *et al.* [56], using X-Ray photoelectronic spectroscopy (XPS). Let us note that using *SD* as a comparative value makes sense, but it does not distinguish between the groups available at the external surface of the CNCs from the internal ones not accessible for subsequent reaction [57], nor does it provide information on the OH groups conformation and reactivity [58]. *SD* defined as such cannot reach 100%. Finally, whatever the CNC used or the ultrasonication treatment, a similar ζ-potential (~ - 48 mV), characterizing the particle charge density, was measured for ultrasonicated particles (Supporting Information, Table S1), close to the value obtained by Zhong *et al.* [59].

3.2 Structural properties

Figure 2 shows a TEM image of a spray-dried CNC suspension after ultrasonication at P = 50 W and E = 10,000 J/g_{CNC}, with ϕ = 0.001 wt%. Spray-dried CNC nanorods in Figure 2 have an average length L_0 ~ 165 nm and diameter d_0 ~ 13 nm, corresponding to an aspect ratio p_0 ~ 12.5: these values are similar to those of freeze-dried samples (for any level of ultrasonication) and close to the values obtained by Lenfant *et al.* [42]. The ultrasonication method used in this work does not break nanoparticles, in disagreement with the finding of Csiszar *et al.* [29]. It is worth pointing out that in TEM individual CNCs may be mistaken with very small bundles of CNCs and high resolution atomic force microscope (AFM) would provide more accurate values, according to Uhlig *et al.* [60].

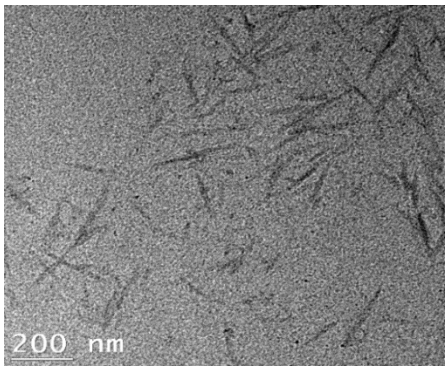

Figure 2: TEM image of a spray-dried CNC suspension.

Figure 3 presents optical micrographs for a spray-dried CNC suspension ultrasonicated at P = 10 W and E = 10,000 J/g_{CNC}, with ϕ = 3-7 wt%. As the CNC concentration increases the polarized light intensity increases from none at ϕ = 3 wt% (isotropic, Figure 3.a) to full iridescence at ϕ = 7 wt% (Figure 3.c) [43], characteristic of the anisometric behavior of the suspension and in agreement with the chiral nematic structure adopted by CNCs [35]. Moreover, some agglomerates of a few micrometers are clearly observed in Figure 3.b. These suggest a double structuration of CNCs in aqueous suspensions: i) at the microscale, there are some agglomerates while ii) at the nanoscale, the orientation of CNC nanoparticles leads to iridescence of the suspension.

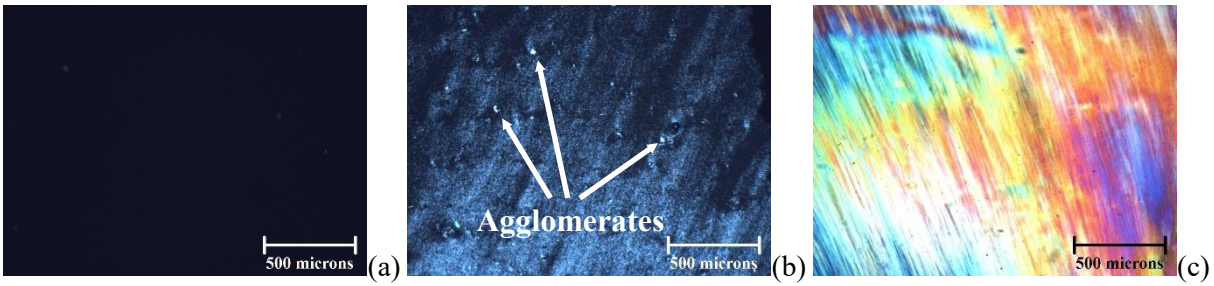

Figure 3: Optical micrographs for spray-dried CNC suspensions ultrasonicated at P = 10 W and E = 10,000 J/g_{CNC} with ϕ = 3 wt% (a), 5 wt% (b) and 7 wt% (c).

Figure 4 presents optical micrographs of spray-dried (a-c) and freeze-dried (d-f) 4 wt% CNC suspensions, respectively, after different ultrasonication treatments. A double structure is also observed in Figure 4, with very bright points and diffuse iridescence, due to agglomerates and nanostructuration of CNCs, respectively. The fingerprint texture of CNC agglomerates seen in Figure 4.d could be related to a local chiral nematic structure [35]. Increased ultrasonication power or energy leads to the break-up of agglomerates in single particles. For a same total energy, the break-up of agglomerates is clearly more efficient for the power of P = 50 W (Figures 4.b and e) compared to P = 10 W (Figures 4.a and d). These phenomena are observable for spray-dried CNC suspensions (Figures 4.a-c), but they are more intense for the freeze-dried CNC suspensions (Figures 4.d-f).

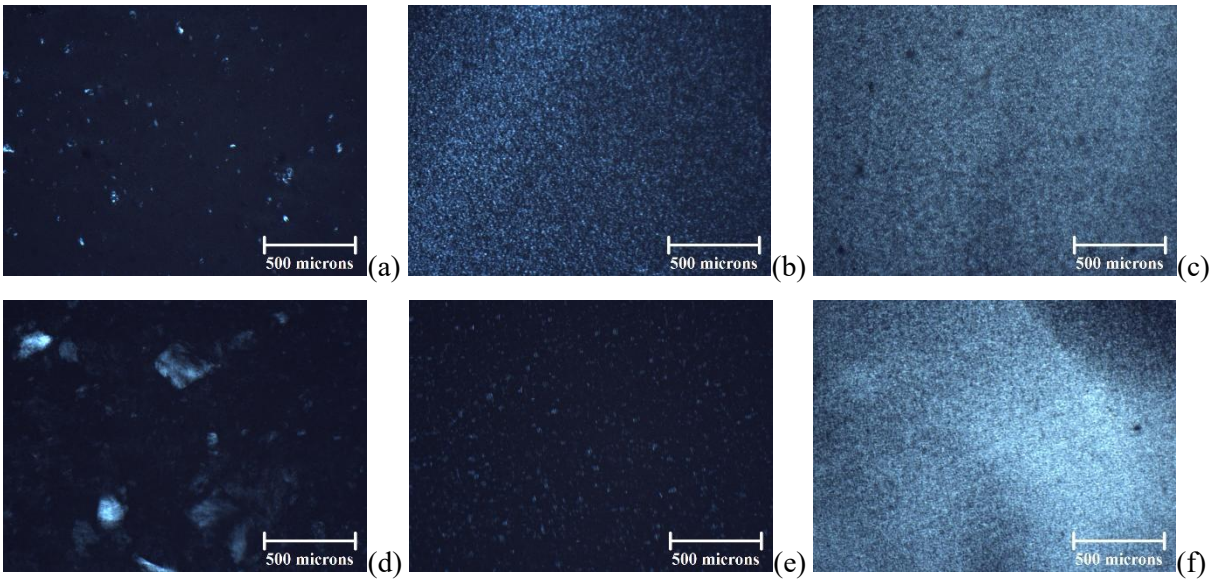

Figure 4: Optical micrographs of a spray-dried (a-c) and freeze-dried (d-f) 4 wt% CNC suspension after ultrasonication at P = 10 W and E = 5,000 J/g_{CNC} (a); at P = 50 W and E = 5,000 J/g_{CNC} (b); P = 50 W and E = 10,000 J/g_{CNC} (c); P = 10 W and E = 2,500 J/g_{CNC} (d); P = 50 W and E = 2,500 J/g_{CNC} (e) and P = 50 W and E = 10,000 J/g_{CNC} (f).

Figure 5 reports the particle equivalent hydrodynamic diameter (d) distributions of CNC particles for spray-dried (a and b) and freeze-dried (c and d) suspensions, respectively, in intensity (a, c) and number (b, d), following different ultrasonication treatments. The light intensity diffused by larger particles is more important and the intensity-based size distribution (Figure 5.a and c) tends to highlight the larger CNC particles in suspension. These data are then used to determine the number-based distributions (Figure 5.b and d). Figure 5.a and c show large particles (d > 100 nm), especially for low ultrasonication in terms of power and/or energy. By increasing both ultrasonication power and energy, the curves shift towards smaller hydrodynamic diameters, confirming that ultrasonication breaks large particles or agglomerates, in agreement with the optical microscope observations of Figure 4. However, the number size distributions indicate a larger number of small particles, with diameters close to a few tens of nanometers (Figure 5.b and d). Ultrasonication does not have the same effect on spray-dried (Figure 5.a and b) and freeze-dried (Figure 5.c and d) suspensions, and the diameter decrease is clearer for the freeze-dried CNC suspensions.

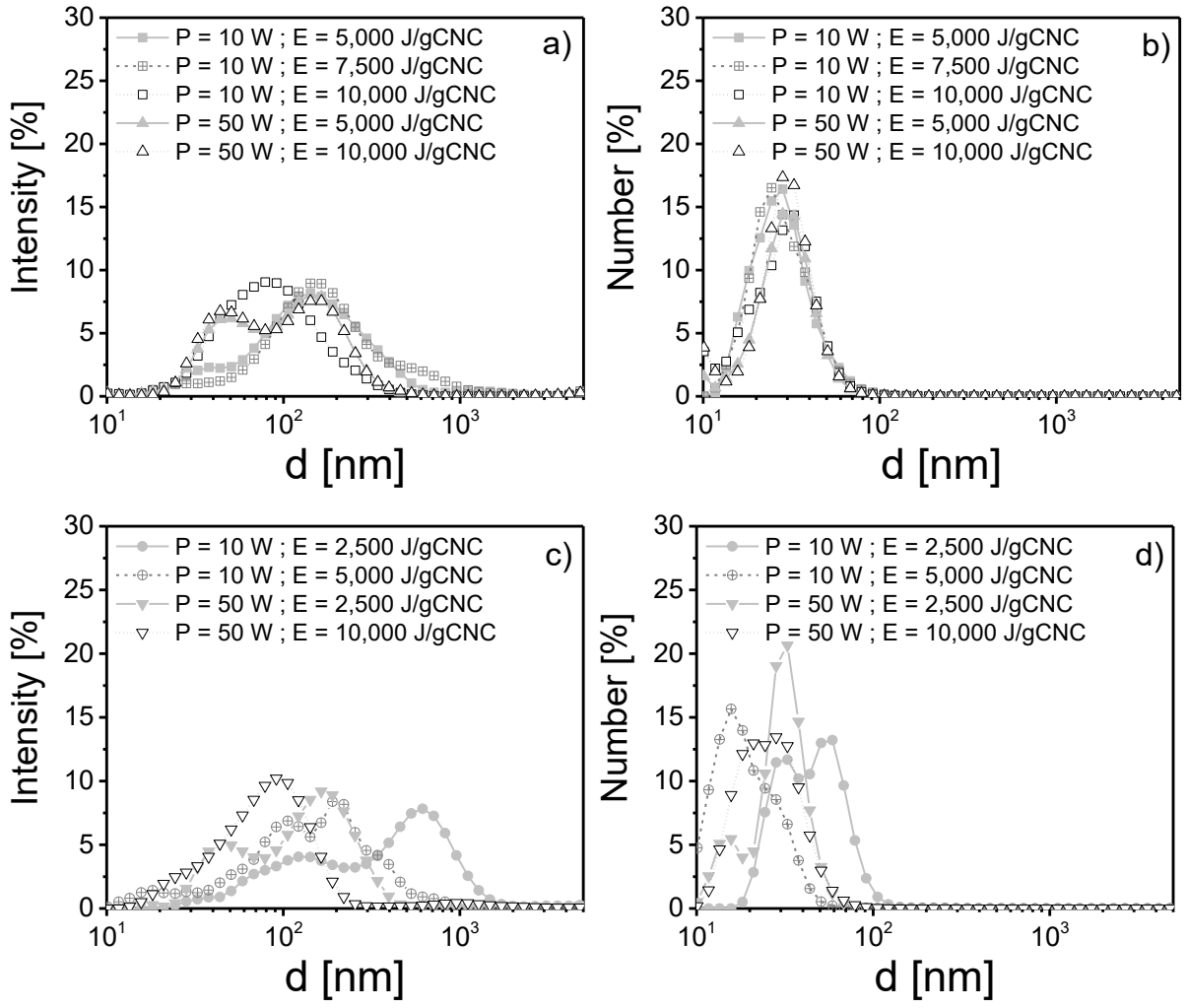

Figure 5: Hydrodynamic CNC diameter distributions in intensity (a, c) and number (b, d) for spray-dried (a, b) and freeze-dried (c, d) suspensions.

Figure 6 presents the *Z*-average hydrodynamic mean diameter of CNC particles and the polydispersity index D_v/D_n as a function of ultrasonication energy for spray-dried (a) and freeze-dried (b) CNC suspensions ultrasonicated at P = 10 and 50 W. Overall, the *Z*-average diameter and polydispersity index decrease with both power and energy of ultrasonication and clearly reach the same limiting values for spray-dried (Figure 6.a) and freeze-dried (Figure 6.b) CNC particles. Moreover, the power seems to be the main parameter governing this decrease. For both power values (P = 10 and 50 W), the minimum *Z*-average diameter of the CNC particles is ~ 75 nm (in agreement with the value measured by Beck *et al.* [9]) and the polydispersity index reaches ~ 2 for both the spray-dried and freeze-dried suspensions at E = 10,000 J/$g_{CNC.}$ The theoretical equivalent hydrodynamic diameter D_z can be calculated from the Stokes-Einstein relation:

$$D_z = \frac{k_B T}{3\pi\eta_s D_t} \quad (4)$$

where k_B, T, η_s and D_t are the Boltzmann constant, the temperature, the solvent viscosity and the translational diffusion coefficient, respectively. As used by de Souza Lima *et al.* [61] for CNCs, the translational diffusion coefficient D_t is written for rod-like shaped particles [62,63]:

$$D_t = \frac{k_B T}{3\pi\eta_s L_0}\left[\delta - 0.5(\gamma\| + \gamma_\perp)\right] \quad (5)$$

with $$\delta = \ln(2L_0 / d_0)$$

and $$\gamma\| = 0.807 + 0.15/\delta + 13.5/\delta^2 - 37/\delta^3 + 22/\delta^4$$

$$\gamma_\perp = -0.193 + 0.15/\delta + 8.1/\delta^2 - 18/\delta^3 + 9/\delta^4$$

Recently, in the case of CNCs, Fraschini *et al.* [64] proposed to modify the translational diffusion coefficient D_t using the Perrin factor S [65] for cylinder-shaped particles:

$$D_t = \frac{k_B T}{3\pi\eta_s L_0} S \quad (6)$$

with $$S = \sqrt[3]{\frac{2}{3}(L_0/d_0)}(f/f_{0)})^{-1}$$

and

$$f/f_0 = 1.009 + 0.01395\ln(L_0/d_0) + 0.0788\ln(L_0/d_0)^2 + 0.00604\ln(L_0/d_0)^3$$

Taking the average dimensions of CNC nanoparticles measured by TEM (L_0 ~ 165 nm and d_0 ~ 13 nm) and considering the influence of the electrostatic double layer thickness (K^{-1}= 3.5 nm, (x 2)) on the effective diameter in aqueous suspensions, D_z = 79.9 nm and D_z = 66.3 nm (Eq.4), using Eq.5 and Eq.6 for D_t, respectively. These theoretical values are in good agreement with the *Z*-average limiting value measured by DLS (~ 75 nm). In the case of ultrasonicated suspensions at P = 50 W, these plateau values are obtained at lower energies (between 2,500 and 5,000 J/g_{CNC}). Finally, it is worth pointing out that the initially increasing values reported for the spray-dried CNC suspension ultrasonicated at P = 10 W when E is increased from 5,000 J/g_{CNC} to 7,500 J/g_{CNC} (Figure 6.a) suggest difficulties to perfectly control the CNC dispersion state and particle size homogeneity at a low ultrasonication power.

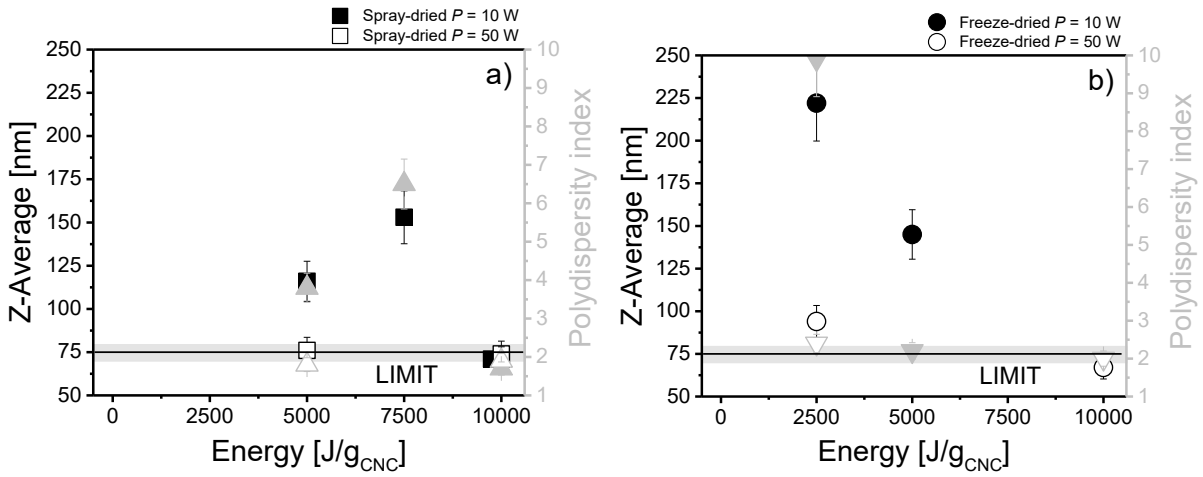

Figure 6: *Z*-average hydrodynamic diameter (in black) and polydispersity index (in red) as a function of ultrasonication energy for spray-dried (a) and freeze-dried (b) CNC suspensions ultrasonicated at P = 10 (open symbols) and 50 W (filled symbols). The grey area represents the error bar corresponding to the limiting values.

In the case of the spray-dried CNC suspensions, ultrasounds seem to gradually erode a few large agglomerates, in agreement with a less marked size decreases observed in the DLS data (Figures 5 and 6). However, the break-up of regular size agglomerates occurs for freeze-dried CNC suspensions, down to individual CNCs or very small bundles. For the same power, higher energy seems to be necessary to achieve the dispersion of spray-dried CNCs.

3.3 Rheological properties

The rheological behavior of aqueous suspensions (in the semi-dilute regime $\phi < \phi_{gelation}$) is presented and discussed in this section. Figure 7 shows the elastic *G'* (a) and loss *G"* (b) moduli as functions of angular frequency and the complex η^* and shear η viscosities (c) as functions of angular frequency ω or shear rate $\dot{\gamma}$, for spray-dried 0 - 5 wt% CNC suspensions ultrasonicated at P = 50 W and E = 10,000 J/g$_{CNC}$. No significant elastic modulus could be measured for the suspensions containing less than 4 wt% CNCs and *G'* (Figure 7.a) is smaller than *G"* (Figure 7.b) over the whole frequency range, as expected for a liquid-like behavior. For suspensions containing less than 4 wt% CNCs a Newtonian behavior is observed at low frequencies (Figure 7.c), characterized by η_0. The suspensions containing 4 and 5 wt% CNCs exhibit a viscoelastic behavior with slight shear-thinning viscosity curves at low frequencies

and shear rates, followed by a pseudo Newtonian plateau η_0 (Figure 7.c) at intermediate frequencies and shear rates. Similar results have already been reported in the literature [30,36], and the suspension behavior shifts from isotropic (ϕ = 1–3 wt%) to lyotropic liquid crystal behavior (ϕ = 4 - 5 wt%), due to the chiral nematic structure of CNCs, in agreement with the onset of iridescence (Figure 3). Moreover, the Cox-Merz rule is not valid for lyotropic liquid crystal (Figure 7.c), as mentioned by Urena Benavides *et al.* [43]. Finally, for all suspensions, the orientation of CNCs in the flow direction leads to another shear-thinning behavior above a critical shear rate $\dot{\gamma}_c$, quasi-independent of volume fraction.

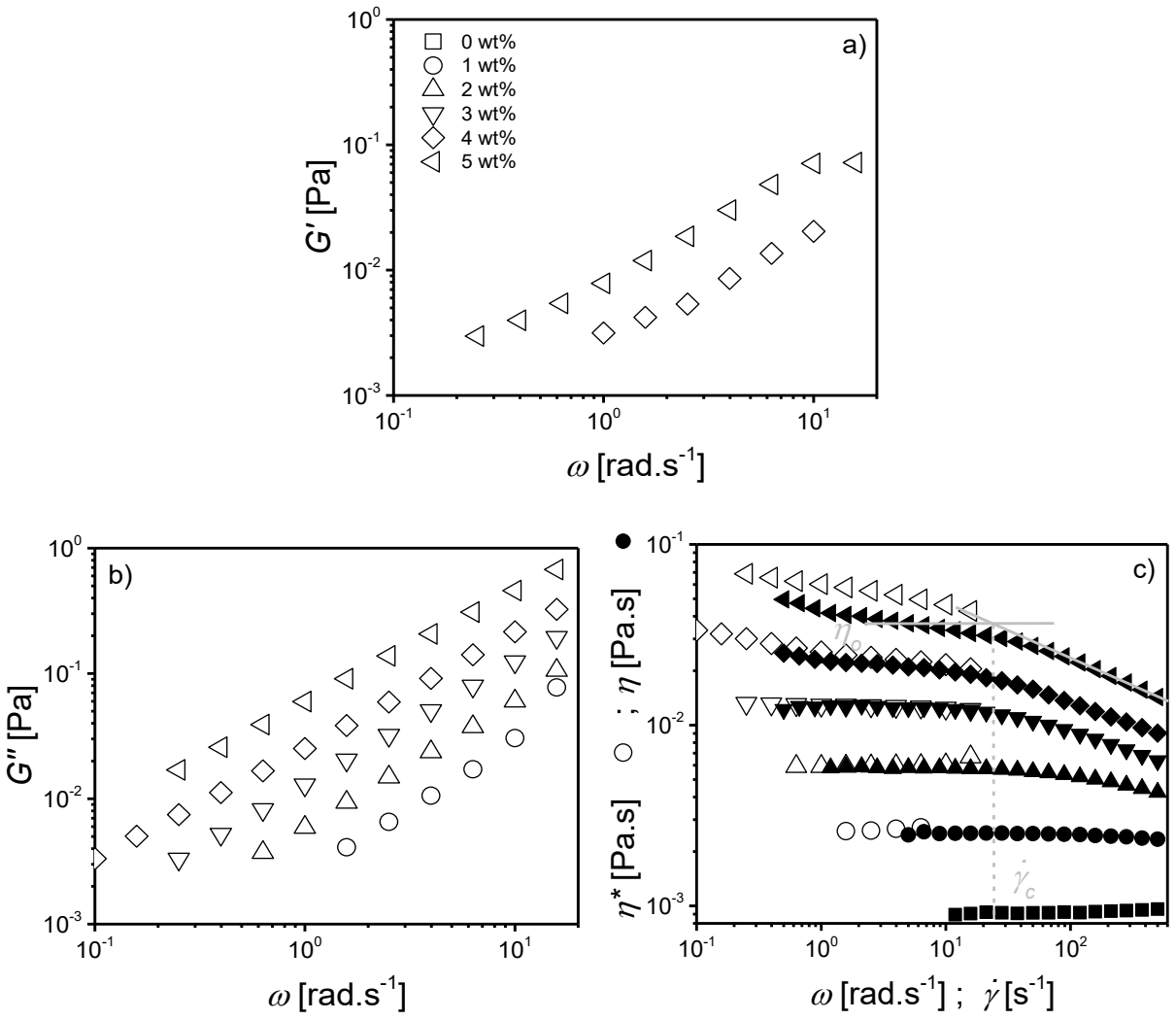

Figure 7: Elastic modulus *G'* (a), loss modulus *G"* (b) and complex and shear viscosities (c) as functions of angular frequency (open symbols) and shear rate (filled symbols) for spray-dried 0-5 wt% CNC suspensions ultrasonicated at P = 50 W and E = 10,000 J/g_{CNC}.

The critical shear rate $\dot{\gamma}_c$ was estimated for both spray and freeze-dried samples after different ultrasonication treatments from viscosity data presented in the supporting

information (Supporting Information, Figure S1). The Péclet number, Pe, characterizes the balance between the Brownian motion and hydrodynamic forces. Pe = 1 corresponds to the limit between Newtonian plateau (Pe <1) and shear thinning due to particle orientation in the flow direction (Pe >1). In the case of rod-like particles of aspect ratio p, the rotational Péclet number, Pe_{rot} is defined by [32] :

$$Pe_{rot} = \frac{\dot{\gamma}\pi\eta_s L^3}{3k_B T(\ln p - 0.8)} \qquad (7)$$

where η_s is the viscosity of the solvent, L the particle length, k_B the Boltzmann constant and T the temperature. Pe_{rot} = 1 corresponds to the critical shear rate, $\dot{\gamma}_c$ and Figure 8 plots the variation of $\dot{\gamma}_c$ as a function of the ultrasonication energy for spray-dried (a) and freeze-dried CNC suspensions ultrasonicated at P = 10 and 50 W. For both spray-dried and freeze-dried CNCs, the critical shear rate $\dot{\gamma}_c$ increases and seems to tend towards the same limiting value with increasing energy, especially when the power is high (Figure 8). Using Eq. 7, the increase of $\dot{\gamma}_c$ for Pe_{rot} = 1 is related to the decrease of L and the increase of p with agglomerate break-up, and can be related to DLS measurements of Figure 6. However, assuming that p = 12.5, the limiting value of $\dot{\gamma}_c \sim 25\ s^{-1}$ leads to $L \sim 650$ nm, which is three times larger than CNC length measured from TEM images ($L \sim 165$ nm, Figure 2). This suggests that $\dot{\gamma}_c$, corresponding to Pe_{rot} = 1, is graphically underestimated and p is overestimated by TEM and does not consider the larger effective diameter of CNC particles in water (~ 20 nm) due to their electrostatic double layer thickness characterized by the Debye length K^{-1}= 3.5 nm.

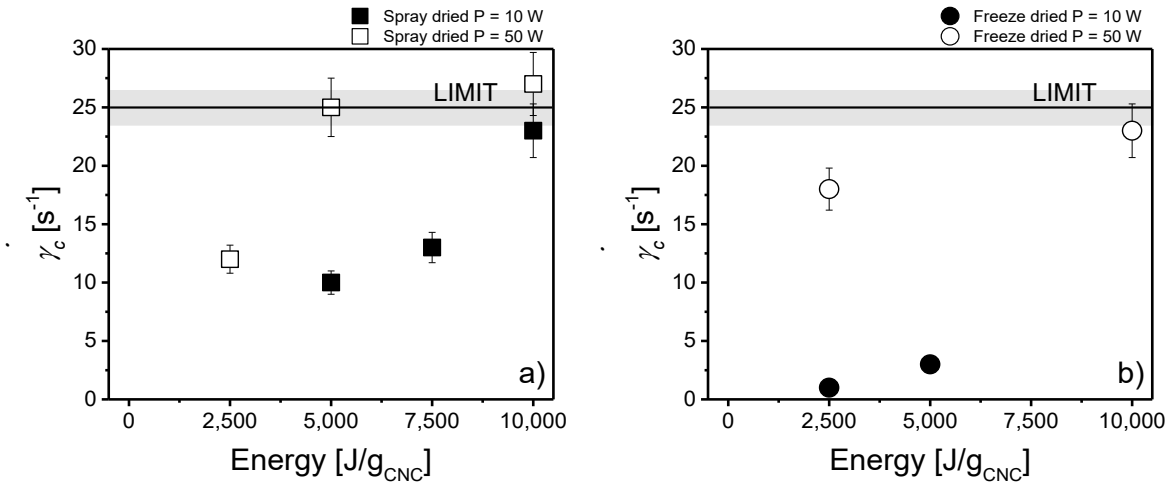

Figure 8: Critical shear rate $\dot{\gamma}_c$ as a function of ultrasonication energy for spray-dried (a) and freeze-dried (b) CNC suspensions ultrasonicated at P = 10 and 50 W. The grey area represents the error bar corresponding to the limiting value.

Figure 9 presents the relative viscosity η_r, defined as the ratio of the pseudo Newtonian plateau or the Newtonian viscosity η_0 of the suspensions, depending on the CNC concentration (Supporting Information, Figure S1), to that of water, as a function of CNC concentration c (g.mL^{-1}) for spray-dried (a) and freeze-dried (b) CNC suspensions following various ultrasonication treatments. The experimental data of Figure 9 are fitted with the Fedors model [46], used for suspensions in dilute and semi-dilute regimes in the presence of agglomerates, defined by:

$$\frac{1}{2(\sqrt{\eta_r}-1)} = \frac{1}{c[\eta]} - \frac{1}{c_m[\eta]} \quad (8)$$

with $c = \frac{\phi}{1-\phi}\rho_{eau}$ in g.mL^{-1}; c_m the maximum packing concentration and $[\eta]$ the intrinsic viscosity in mL.g^{-1} equal to the sum of the rigid body $[\eta]_0$ and the electroviscous $[\eta]_{el}$ contributions of particles [49,66].

Assuming p = 12.5 for all suspensions and using the following Simha relation for nanorods [67] validated by Boluk *et al.* [40] in the case of CNCs:

$$[\eta]_0 = \frac{14}{15} + \frac{p^2}{15(\ln 2p - 1.5)} + \frac{p^2}{5(\ln 2p - 0.5)} \quad (9)$$

we obtain $[\eta]_0 \sim 18.5 = 12$ mL.g^{-1} (changing the CNC concentration in g.mL^{-1}). The values for c_m, and $[\eta] = [\eta]_0 + [\eta]_{el}$ (in mL.g^{-1}) are listed in Table 1 for all suspensions.

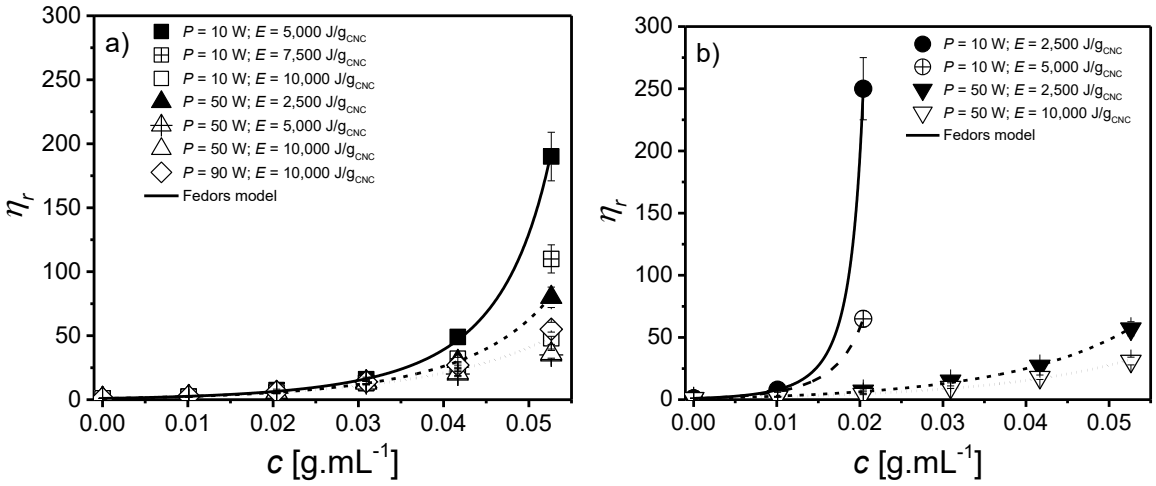

Figure 9: Relative viscosity η_r as a function of concentration for spray-dried (a) and freeze-dried (b) CNC suspensions. Lines correspond to the Fedors model fits.

Table 1. Maximum concentration c_{max} and intrinsic viscosity $[\eta]$ for CNC suspensions

CNCs	Power (W)	Energy (J/g_{CNC})	Fedors model			
			c_m ($g.mL^{-1}$)	$[\eta] = [\eta]_0 + [\eta]_{el}$ ($mL.g^{-1}$)		
				$[\eta]$	$[\eta]_0$	$[\eta]_{el}$
Spray-dried	10	5,000	0.067	105	12	93
		7,500	0.075	100		88
		10,000	~ 0.11			
	50	2,500	0.075	100		88
		5,000	~ 0.11			
		10,000				
	90	10,000	~ 0.11	100		88
Freeze-dried	10	2,500	0.024	210		198
		5,000	0.029	200		188
	50	2,500	0.103	110		98
		10,000	~ 0.11	100		88

For all suspensions, η_r increases with c up to a maximum packing concentration c_m where η_r tends towards infinity, a trend especially visible in the case of freeze-dried suspensions that have been weakly ultrasonicated. Moreover, c_m increases and $[\eta]_{el}$ (or $[\eta]$) decreases with increasing ultrasonication power or energy (Table 1). These values are in agreement with those reported in the literature [49]. The decrease of the particle size (Figure 6) leads to decreased suspension viscosity and increased c_m, until a same maximum value ($c_{m\,max} \sim 0.11$), for both spray and freeze-dried suspensions, in agreement with the same limiting

size measured by DLS (Figure 6). Finally, Figure 10 presents a master curve of η_r as a function of c/c_m. This master curve can also be fitted by Fedors model substituting c by $c_{eff} = 0.11\ c/c_m$.

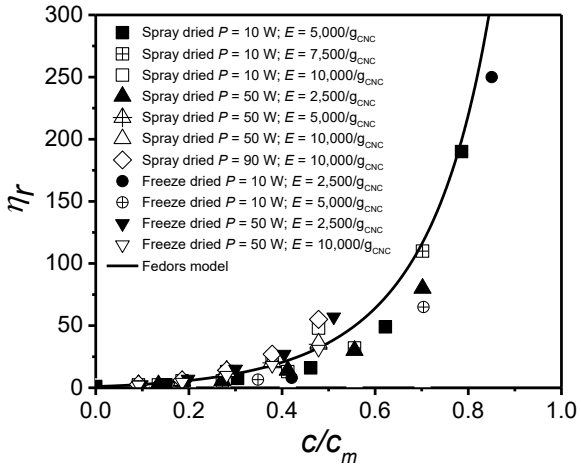

Figure 10: Master curve for the relative viscosity, η_r, as a function of concentration c reduced by the maximum packing concentration c_m. The line corresponds to the fit of the Fedors model.

To summarize, spray- and freeze-dried CNCs have the same number of sulfate half ester groups measured by EDX. The same optimal dispersion state can clearly be reached for both CNC types, as illustrated by hydrodynamic diameter measurements and rheological properties. Increased power and energy of ultrasonication decrease particle size by breaking agglomerates into single nanoparticles or very small bundles, as observed with optical microscopy and dynamic light scattering measurements. This particle size decrease is correlated to a maximum packing concentration increase and an intrinsic viscosity reduction. Spray-dried CNCs require more energy to achieve their maximum dispersion in water. Moreover, ionic conductivity measurements suggest an increase of the average number of ionic groups available in the aqueous suspensions.

4. Discussion

Because no decrease of the S/C ratio is observed by EDX (Figure 1) after a strong ultrasonication and dialysis (which would have removed free ions), we conclude that all O-SO_3H groups remain attached to the spray- and freeze-dried CNC surface. This result clearly demonstrates the absence of desulfation under ultrasonication, often reported as possible [38]. Thermodynamics support this result as well. Indeed, the maximum energy released as work during ultrasonication can be estimated as $E \sim 5{,}500\ \text{kJ.kg}^{-1} = 100\ \text{kJ.mol}^{-1}$. This calculation is

based on the implosion of a cavitation vapor bubble from maximum temperature T = 1,000 °C and pressure P = 40 MPa to ambient conditions, with an enthalpy and speed losses of Δh ~ 4,400 kJ.kg^{-1} and Δv ~ 1,500 m.s^{-1}, respectively. An energy of 100 kJ.mol^{-1} is not sufficient to break O-S covalent bonds [24], characterized by E ~ 500 kJ.mol^{-1} [68]. On the other hand, increase of the energy or power of ultrasonication breaks agglomerates in individual nanoparticles or very small bundles, down to the same limiting hydrodynamic diameter (~ 75 nm, Figure 6) for both spray- and freeze-dried CNCs. The maximum critical shear rate (Figure 8) and the minimum reduced viscosity (Figure 9) values correspond to the maximum dispersion state of CNCs in water reported for both spray and freeze-dried suspensions, hence, probably related to the substitution degree on CNC surface, controlled by sulfuric acid hydrolysis conditions [4]. The break-up of the smallest agglomerates observed by optical microscopy (Figures 4.a-c) and measured by DLS in the case of spray-dried CNC suspensions (Figures 5.a and b) is not favored because of their high cohesion strength (in the range of 10^4 – 10^9 Pa for agglomerates diameter ranging from 50 to 0.5 µm without porosity. The cohesion strength could decrease by two decades for high porosity [21]). The less inter-agglomerated macroporous structure (pore size > 1 µm) of spray-dried CNCs (characterized by an higher powder bulk density) could favor the formation of smaller agglomerates. That morphology would reduce water absorption inside large agglomerates and decelerate break-up in the first minutes of ultrasonication; this could however be adjusted by changing the spray-drying conditions [20]. The dispersion mechanism occurring during ultrasonication, based on cavitation, can overcome the hydrogen and/or van der Waals bonds between CNCs with binding energy on the order of 10 kJ.mol^{-1} [17,21,69] (below the maximum energy released by cavitation E ~ 100 kJ.mol^{-1}). Time or total energy applied during ultrasonication controls the number of implosions [28], but the instantaneous efficiency of cavitation is as low as the power is weak, according to the relation between the amplitude imposed and the bubble volume generated [23]. For the same lower energy (E < 5,000 J/g$_{CNC}$), the use of P = 50 W enhances the CNC dispersion compared to P = 10 W. Moreover, we need to mention that before ultrasonication, the viscosity of spray-dried CNC aqueous suspensions is lower (close to that of water) than that of freeze-dried CNC suspensions. This could favor cavitation, especially in the case of a low ultrasonication power. Finally, based on the conditions used by Peng et al. [70] for spray- and freeze-drying a 2 wt% CNC suspension, we can estimate the energy required to dry 1 g of CNC (and thus remove 49 g of water), neglecting the residual moisture. The average specific heat capacities of cellulose (Cp_{CNC} = 1 J.g^{-1}.°C^{-1} [71]), liquid water ($Cp_{water\text{-}liq}$ = 4.2 J.g^{-1}.°C^{-1} [72]) and solid water ($Cp_{water\text{-}sol}$ = 2.1 J.g^{-1}.°C^{-1} [72]) were

used to calculate the energy required to bring the suspension temperature from 20 °C to drying temperatures. The water enthalpy of vaporization at 90 °C (outlet temperature in the spray-dryer), ΔH_{vap} = 2283 J.g^{-1} [73], that of freezing at 0 °C, ΔH_{fre} = 335 J.g^{-1} [74], and that of sublimation at -80 °C (temperature in the freeze dryer), ΔH_{sub} = 2830 J.g^{-1} [75] not significantly dependent on the pressure, were taken to determine the energy needed for the water phase transformations. This thermodynamic approach yields energy requirements around 126 and 168 kJ/g_{CNC} (or 2.6 and 3.4 kJ per g of water removed) for spray- and freeze-drying processes, respectively. The ratio of these energy requirements is roughly the same order of magnitude as compared to values taken from examples in the food industry [74] (spray-drying consumes about 3.5 - 5 kJ per g of water removed while freeze-drying consumes more than 6 kJ per g of water removed). If spray-dried CNCs required a little more ultrasonication energy to achieve their dispersion in water, this drying process is clearly less energy consuming, encouraging its development.

The decrease of the relative viscosity shown in Figure 9 of CNC suspensions is correlated with the decrease of the particle size observed by DLS (Figure 6) as already reported in the literature [38], but it contradicts theories generally used for electrostatically stabilized colloidal suspensions of rigid particles [32]. It also apparently contradicts the mechanism proposed by Beck *et al.* [24] based on ejected ions from the bound-water layer (explaining the ionic conductivity increase after ultrasonication), which is supposed to increase the electrostatic double layer thickness. Indeed, in the case of electrostabilized hard spheres, a particle size decrease or a thicker electrostatic layer (for example due to a lower ionic strength) leads to an higher apparent volume occupied by particles and their electrostatic double layer [31], amplifying electroviscous effects [55,76]. Since the same charge density was measured for all suspensions (ζ-potential ~ 48 mV – Supporting Information, Table S1) and the particle size decreased after strong ultrasonication, the reduction of the viscoelastic properties could be related to the ionic strength I, hence, to a thinner electrostatic double layer [41]. In our case, we suggest that these ions were probably trapped with water inside agglomerates before ultrasonication and released after agglomerate break-up. It may reduce the thickness of the electrostatic double layer [49], in agreement with the decrease of $[\eta]_{el}$ reported in Table 1, especially as the agglomerate break-up probably increases the CNC aspect ratio and the rigid body contribution $[\eta]_0$. In the same way, large porous CNC agglomerates can trap water, which increases the apparent CNC concentration. These arguments could explain the important viscosity increases shown in Figure 9 in the presence

of large agglomerates, in agreement with the drastic c_m decreases reported in Table 1. In other words, the ions and water released in water by breaking agglomerates prevent CNC gelation.

5. Conclusion

The optimal dispersion state attainable for spray-dried cellulose nanocrystals (CNCs) in water is comparable to that of freeze-dried CNCs, (mean hydrodynamic diameter ~ 75 nm). In aqueous suspensions, ultrasonication improves their dispersion state by breaking agglomerates without demonstrably causing desulfation (as many had previously hypothesized). Ultrasonication efficiency, based on cavitation, is strongly dominated by the power level (even more than energy) of the probe, which must be high to favor CNC dispersion. This consideration is often obscured in the literature. Moreover, spray-dried CNCs need more energy than their freeze-dried counterparts to achieve maximum dispersion in water. However, the energy required for the spray-drying process compared to freeze-drying favors the use of spray-dried CNCs. As the dispersion state of CNC is improved, rheological properties show increases of the critical shear-rate (shear rate above which shear-thinning is observed) and the maximum packing concentration until the same limiting values of 25 s^{-1} and 0.11 $g.mL^{-1}$, respectively, for both well dispersed spray- and freeze-dried CNC suspensions. Agglomerates break-up releases both ions and water in suspensions, preventing gel formation. The relationships between structure and rheology have been demonstrated using the Péclet number and Fedors model, based on intrinsic viscosity and maximum packing concentration, leading to a master curve representation of the various systems/conditions. This study highlights processing considerations for the optimal dispersion and use of spray-dried cellulose nanocrystals, and demonstrates the interest of rheology as a tool to characterize these complex colloidal suspensions.

6. Acknowledgments

FPInnovations and CelluForce are acknowledged for providing the freeze-dried and spray-dried CNCs, respectively. We also thank NSERC, PRIMA Québec and FPInnovations for their financial support. The authors are grateful to Dr. Wadood Hamad of FPInnovations for his helpful suggestions. Finally, we would like to mention the help of Mr. Philippe Massé

with TEM observations, Prof. Daria Camilla Boffito with ultrasonication and Mr. Valentin Ponce with rheometry.

7. References

[1] S.J. Eichhorn, A. Dufresne, M. Aranguren, N.E. Marcovich, J.R. Capadona, S.J. Rowan, C. Weder, W. Thielemans, M. Roman, S. Renneckar, W. Gindl, S. Veigel, J. Keckes, H. Yano, K. Abe, M. Nogi, A.N. Nakagaito, A. Mangalam, J. Simonsen, A.S. Benight, A. Bismarck, L.A. Berglund, T. Peijs, Review: current international research into cellulose nanofibres and nanocomposites, J. Mater. Sci. 45 (2010) 1–33. doi:10.1007/s10853-009-3874-0.

[2] G. Siqueira, J. Bras, A. Dufresne, Cellulosic Bionanocomposites: A Review of Preparation, Properties and Applications, Polymers (Basel). 2 (2010) 728–765. doi:10.3390/polym2040728.

[3] R.J. Moon, A. Martini, J. Nairn, J. Simonsen, J. Youngblood, Cellulose nanomaterials review: structure, properties and nanocomposites, Chem. Soc. Rev. 40 (2011) 3941. doi:10.1039/c0cs00108b.

[4] S. Beck-Candanedo, M. Roman, D.G. Gray, Effect of Reaction Conditions on the Properties and Behavior of Wood Cellulose Nanocrystal Suspensions, Biomacromolecules. 6 (2005) 1048–1054. doi:10.1021/bm049300p.

[5] W.Y. Hamad, T.Q. Hu, Structure-process-yield interrelations in nanocrystalline cellulose extraction, Can. J. Chem. Eng. 88 (2010) n/a-n/a. doi:10.1002/cjce.20298.

[6] Y. Habibi, L.A. Lucia, O.J. Rojas, Cellulose Nanocrystals: Chemistry, Self-Assembly, and Applications, Chem. Rev. 110 (2010) 3479–3500. doi:10.1021/cr900339w.

[7] L. Brinchi, F. Cotana, E. Fortunati, J.M. Kenny, Production of nanocrystalline cellulose from lignocellulosic biomass: Technology and applications, Carbohydr. Polym. 94 (2013) 154–169. doi:10.1016/j.carbpol.2013.01.033.

[8] J. Bouchard, M. Méthot, C. Fraschini, S. Beck, Effect of oligosaccharide deposition on the surface of cellulose nanocrystals as a function of acid hydrolysis temperature, Cellulose. 23 (2016) 3555–3567. doi:10.1007/s10570-016-1036-5.

[9] S. Beck, J. Bouchard, R. Berry, Dispersibility in Water of Dried Nanocrystalline Cellulose, Biomacromolecules. 13 (2012) 1486–1494. doi:10.1021/bm300191k.

[10] Long Jiang, E. Morelius, Jinwen Zhang, M. Wolcott, J. Holbery, Study of the Poly(3-hydroxybutyrate-co-3-hydroxyvalerate)/Cellulose Nanowhisker Composites Prepared

by Solution Casting and Melt Processing, J. Compos. Mater. 42 (2008) 2629–2645. doi:10.1177/0021998308096327.

[11] D. Bagheriasl, P.J. Carreau, B. Riedl, C. Dubois, W.Y. Hamad, Shear rheology of polylactide (PLA)–cellulose nanocrystal (CNC) nanocomposites, Cellulose. 23 (2016) 1885–1897. doi:10.1007/s10570-016-0914-1.

[12] K. Ben Azouz, E.C. Ramires, W. Van den Fonteyne, N. El Kissi, A. Dufresne, Simple Method for the Melt Extrusion of a Cellulose Nanocrystal Reinforced Hydrophobic Polymer, ACS Macro Lett. 1 (2012) 236–240. doi:10.1021/mz2001737.

[13] V. Khoshkava, M.R. Kamal, Effect of Surface Energy on Dispersion and Mechanical Properties of Polymer/Nanocrystalline Cellulose Nanocomposites, Biomacromolecules. 14 (2013) 3155–3163. doi:10.1021/bm400784j.

[14] H. Sojoudiasli, M.C. Heuzey, P.J. Carreau, Mechanical and morphological properties of cellulose nanocrystal (CNC)-polypropylene composites, Polym. Compos. (2016) 1–9.

[15] S. Beck, J. Bouchard, Effect of storage conditions on cellulose nanocrystal stability, Tappi J. 13 (2014) 9–17.

[16] M.I. Voronova, A.G. Zakharov, O.Y. Kuznetsov, O. V Surov, The effect of drying technique of nanocellulose dispersions on properties of dried materials, Mater. Lett. 68 (2012) 164–167. doi:10.1016/j.matlet.2011.09.115.

[17] J. Han, C. Zhou, Y. Wu, F. Liu, Q. Wu, Self-Assembling Behavior of Cellulose Nanoparticles during Freeze-Drying: Effect of Suspension Concentration, Particle Size, Crystal Structure, and Surface Charge, Biomacromolecules. 14 (2013) 1529–1540. doi:10.1021/bm4001734.

[18] A. Dufresne, Nanocellulose: a new ageless bionanomaterial, Mater. Today. 16 (2013) 220–227. doi:10.1016/j.mattod.2013.06.004.

[19] T. Javanbakht, W. Raphael, J.R. Tavares, Physicochemical properties of cellulose nanocrystals treated by photo-initiated chemical vapour deposition (PICVD), Can. J. Chem. Eng. 94 (2016) 1135–1139. doi:10.1002/cjce.22473.

[20] Peng Y., Yousoo H., Gardner J.D., Y. Peng, H. Yousoo, D.J. Gardner, Spray-drying cellulose nanofibrils: effect of drying process parameters on particle morphology and size distribution, Wood Fiber Sci. 44 (2012) 1–14.

[21] V. Khoshkava, M.R.R. Kamal, Effect of drying conditions on cellulose nanocrystal (CNC) agglomerate porosity and dispersibility in polymer nanocomposites, Powder Technol. 261 (2014) 288–298. doi:10.1016/j.powtec.2014.04.016.

[22] P. Lu, Y.-L. Hsieh, Preparation and properties of cellulose nanocrystals: Rods, spheres, and network, Carbohydr. Polym. 82 (2010) 329–336. doi:10.1016/j.carbpol.2010.04.073.

[23] B.E.E. Noltingk, E.. A. Neppiras, Cavitation produced by Ultrasonics, Proc. Phys. Soc. Sect. B. 63 (1950) 674–685. doi:10.1088/0370-1301/63/9/305.

[24] S. Beck, J. Bouchard, R. Berry, Controlling the Reflection Wavelength of Iridescent Solid Films of Nanocrystalline Cellulose, Biomacromolecules. 12 (2011) 167–172. doi:10.1021/bm1010905.

[25] Z. Lu, L. Fan, H. Zheng, Q. Lu, Y. Liao, B. Huang, Preparation, characterization and optimization of nanocellulose whiskers by simultaneously ultrasonic wave and microwave assisted, Bioresour. Technol. 146 (2013) 82–88. doi:10.1016/j.biortech.2013.07.047.

[26] Y. Cao, P. Zavattieri, J. Youngblood, R. Moon, J. Weiss, The relationship between cellulose nanocrystal dispersion and strength, Constr. Build. Mater. 119 (2016) 71–79. doi:10.1016/j.conbuildmat.2016.03.077.

[27] X.M. Dong, J.-F. Revol, D.G. Gray, Effect of microcrystallite preparation conditions on the formation of colloid crystals of cellulose, Cellulose. 5 (1998) 19–32. doi:10.1023/A:1009260511939.

[28] S. Sumari, A. Roesyadi, S. Sumarno, Effects of ultrasound on the morphology, particle size, crystallinity, and crystallite size of cellulose, Sci. Study Res. Chem. Chem. Eng. Biotechnol. Food Ind. 14 (2013) 229–239.

[29] E. Csiszar, P. Kalic, A. Kobol, E.D.P. Ferreira, The effect of low frequency ultrasound on the production and properties of nanocrystalline cellulose suspensions and films, Ultrason. Sonochem. 31 (2016) 473–480. doi:10.1016/j.ultsonch.2016.01.028.

[30] S. Shafiei-Sabet, W.Y. Hamad, S.G. Hatzikiriakos, Rheology of Nanocrystalline Cellulose Aqueous Suspensions, Langmuir. 28 (2012) 17124–17133. doi:10.1021/la303380v.

[31] F.M. Horn, W. Richtering, J. Bergenholtz, N. Willenbacher, N.J. Wagner, Hydrodynamic and Colloidal Interactions in Concentrated Charge-Stabilized Polymer Dispersions, J. Colloid Interface Sci. 225 (2000) 166–178. doi:10.1006/jcis.1999.6705.

[32] J. Mewis, N.J. Wagner, Introduction to colloid science and rheology, in: Colloid. Suspens. Rheol., Cambridge University Press, Cambridge, 2011: pp. 1–35. doi:10.1017/CBO9780511977978.004.

[33] M.M. de Souza Lima, R. Borsali, Rodlike Cellulose Microcrystals: Structure,

Properties, and Applications, Macromol. Rapid Commun. 25 (2004) 771–787. doi:10.1002/marc.200300268.

[34] S.-L. Tseng, A. Valente, D.G. Gray, Cholesteric liquid crystalline phases based on (acetoxypropyl)cellulose, Macromolecules. 14 (1981) 715–719. doi:10.1021/ma50004a049.

[35] J.P.F. Lagerwall, C. Schütz, M. Salajkova, J. Noh, J. Hyun Park, G. Scalia, L. Bergström, Cellulose nanocrystal-based materials: from liquid crystal self-assembly and glass formation to multifunctional thin films, NPG Asia Mater. 6 (2014) e80. doi:10.1038/am.2013.69.

[36] M. Bercea, P. Navard, Shear Dynamics of Aqueous Suspensions of Cellulose Whiskers, Macromolecules. 33 (2000) 6011–6016. doi:10.1021/ma000417p.

[37] J. Araki, M. Wada, S. Kuga, T. Okano, Influence of surface charge on viscosity behavior of cellulose microcrystal suspension, J. Wood Sci. 45 (1999) 258–261. doi:10.1007/BF01177736.

[38] S. Shafeiei-Sabet, W.Y. Hamad, S.G. Hatzikiriakos, S. Shafiei-Sabet, W.Y. Hamad, S.G. Hatzikiriakos, S. Shafeiei-Sabet, W.Y. Hamad, S.G. Hatzikiriakos, S. Shafiei-Sabet, W.Y. Hamad, S.G. Hatzikiriakos, Influence of degree of sulfation on the rheology of cellulose nanocrystal suspensions, Rheol. Acta. 52 (2013) 741–751. doi:10.1007/s00397-013-0722-6.

[39] K.J. Le Goff, C. Gaillard, C. Garnier, T. Aubry, Electrostatically driven modulation of the reinforcement of agarose hydrogels by cellulose nanowhiskers, J. Appl. Polym. Sci. 133 (2016) n/a-n/a. doi:10.1002/app.43063.

[40] Y. Boluk, R. Lahiji, L. Zhao, M.T. McDermott, Suspension viscosities and shape parameter of cellulose nanocrystals (CNC), Colloids Surfaces A Physicochem. Eng. Asp. 377 (2011) 297–303. doi:10.1016/j.colsurfa.2011.01.003.

[41] S. Beck, J. Bouchard, Ionic strength control of sulfated cellulose nanocrystal suspension viscosity, Tappi J. 15 (2016) 363–372.

[42] G. Lenfant, M.-C.C. Heuzey, T.G.M. van de Ven, P.J. Carreau, A comparative study of ECNC and CNC suspensions: effect of salt on rheological properties, Rheol. Acta. 56 (2017) 51–62. doi:10.1007/s00397-016-0979-7.

[43] E.E. Ureña-Benavides, G. Ao, V.A. Davis, C.L. Kitchens, Rheology and Phase Behavior of Lyotropic Cellulose Nanocrystal Suspensions, Macromolecules. 44 (2011) 8990–8998. doi:10.1021/ma201649f.

[44] A. Einstein, Berichtigung zu meiner Arbeit: „Eine neue Bestimmung der

Moleküldimensionen", Ann. Phys. 339 (1911) 591–592. doi:10.1002/andp.19113390313.

[45] J.G. Kirkwood, J. Riseman, The Intrinsic Viscosities and Diffusion Constants of Flexible Macromolecules in Solution, J. Chem. Phys. 16 (1948) 565–573. doi:10.1063/1.1746947.

[46] R.F. Fedors, An equation suitable for describing the viscosity of dilute to moderately concentrated polymer solutions, Polymer. 20 (1979) 225–228. doi:10.1016/0032-3861(79)90226-X.

[47] E. González-Labrada, D.G. Gray, Viscosity measurements of dilute aqueous suspensions of cellulose nanocrystals using a rolling ball viscometer, Cellulose. 19 (2012) 1557–1565. doi:10.1007/s10570-012-9746-9.

[48] M.-C. Li, Q. Wu, K. Song, S. Lee, Y. Qing, Y. Wu, Cellulose Nanoparticles: Structure–Morphology–Rheology Relationships, ACS Sustain. Chem. Eng. 3 (2015) 821–832. doi:10.1021/acssuschemeng.5b00144.

[49] G. Lenfant, M.C. Heuzey, T.G.M. van de Ven, P.J. Carreau, Intrinsic viscosity of suspensions of electrosterically stabilized nanocrystals of cellulose, Cellulose. 22 (2015) 1109–1122. doi:10.1007/s10570-015-0573-7.

[50] T. Abitbol, E. Kloser, D.G. Gray, Estimation of the surface sulfur content of cellulose nanocrystals prepared by sulfuric acid hydrolysis, Cellulose. 20 (2013) 785–794. doi:10.1007/s10570-013-9871-0.

[51] K. Makino, H. Ohshima, Electrophoretic mobility of a colloidal particle with constant surface charge density, Langmuir. 26 (2010) 18016–18019. doi:10.1021/la1035745.

[52] A. Palanisami, J.H. Miller, Simultaneous sizing and electrophoretic mobility measurement of sub-micron particles using Brownian motion, Electrophoresis. 31 (2010) 3613–3618. doi:10.1002/elps.201000291.

[53] G. Sposito, The Chemistry of Soils, 2nd Editio, Oxford University Press, Inc., 2008.

[54] G.. Marion, K.L. Babcock, Predicting Specific Conductance and Salt Concentration in Dilute Aqueous Solutions, Soil Sci. 122 (1976) 181–187.

[55] P.C. Hiemenz, R. Rajagopalan, Principles of Colloid and Surface Chemistry, Marcel Dek, 1997.

[56] H. Sojoudiasli, M. Heuzey, P.J. Carreau, B. Riedl, Rheological investigation of CNC and hydrophobic CNC suspensions in polar solventssolvents, (2017).

[57] C. Goussé, H. Chanzy, G. Excoffier, L. Soubeyrand, E. Fleury, Stable suspensions of partially silylated cellulose whiskers dispersed in organic solvents, Polymer. 43 (2002)

2645–2651. doi:10.1016/S0032-3861(02)00051-4.

[58] S. Eyley, W. Thielemans, Surface modification of cellulose nanocrystals, Nanoscale. 6 (2014) 7764–7779. doi:10.1039/C4NR01756K.

[59] L. Zhong, S. Fu, X. Peng, H. Zhan, R. Sun, Colloidal stability of negatively charged cellulose nanocrystalline in aqueous systems, Carbohydr. Polym. 90 (2012) 644–649. doi:10.1016/j.carbpol.2012.05.091.

[60] M. Uhlig, A. Fall, S. Wellert, M. Lehmann, S. Prévost, L. Wågberg, R. Von Klitzing, G. Nyström, Two-Dimensional Aggregation and Semidilute Ordering in Cellulose Nanocrystals, Langmuir. 32 (2016) 442–450. doi:10.1021/acs.langmuir.5b04008.

[61] M.M. De Souza Lima, J.T. Wong, M. Paillet, R. Borsali, R. Pecora, Translational and Rotational Dynamics of Rodlike Cellulose Whiskers, Langmuir. 19 (2003) 24–29. doi:10.1021/la020475z.

[62] S. Broersma, Rotational Diffusion Constant of a Cylindrical Particle, J. Chem. Phys. 32 (1960) 1626–1631. doi:10.1063/1.1730994.

[63] S. Broersma, Viscous Force Constant for a Closed Cylinder, J. Chem. Phys. 32 (1960) 1632–1635. doi:10.1063/1.1730995.

[64] Fraschini, Critical discussion of light scattering and microscopy techniques for CNC particle sizing, Nord. Pulp Pap. Res. J. 29 (2014) 031–040. doi:10.3183/NPPRJ-2014-29-01-p031-040.

[65] F. Perrin, Mouvement Brownien d'un ellipsoide (II). Rotation libre et dépolarisation des fluorescences. Translation et diffusion de molécules ellipsoidales, Le J. Phys. Le Radium. 7 (1936) 1–11.

[66] L. Jowkarderis, T.G.M. van de Ven, Intrinsic viscosity of aqueous suspensions of cellulose nanofibrils, Cellulose. 21 (2014) 2511–2517. doi:10.1007/s10570-014-0292-5.

[67] R. Simha, The Influence of Brownian Movement on the Viscosity of Solutions., J. Phys. Chem. 44 (1940) 25–34. doi:10.1021/j150397a004.

[68] Y.-R. Luo, Handbook of Bond Dissociation Energies in Organic Compounds, CRC Press, 2002. https://books.google.ca/books?id=8CHNBQAAQBAJ&dq=Handbook+of+Bond+Dissociation+Energies+in+Organic+Compounds&lr=&source=gbs_navlinks_s.

[69] J.M. Berg, J.L. Tymoczko, L. Stryer, Biochemistry, W. H. Freeman and Company, 2002. https://www.ncbi.nlm.nih.gov/books/NBK21154/.

[70] Y. Peng, D.J. Gardner, Y. Han, A. Kiziltas, Z. Cai, M.A. Tshabalala, Influence of

drying method on the material properties of nanocellulose I: Thermostability and crystallinity, Cellulose. 20 (2013) 2379–2392. doi:10.1007/s10570-013-0019-z.

[71] H. Krässig, J. Schurz, R.G. Steadman, K. Schliefer, W. Albrecht, M. Mohring, H. Schlosser, Cellulose, in: Ullmann's Encycl. Ind. Chem., Wiley-VCH Verlag GmbH & Co. KGaA, Weinheim, Germany, 2004. doi:10.1002/14356007.a05_375.pub2.

[72] J.P. Briner, Encyclopedia of Snow, Ice and Glaciers, 2011. doi:10.1007/978-90-481-2642-2.

[73] C.O. Popiel, J. Wojtkowiak, Simple Formulas for Thermophysical Properties of Liquid Water for Heat Transfer Calculations (from 0°C to 150°C), Heat Transf. Eng. 19 (1998) 87–101. doi:10.1080/01457639808939929.

[74] N. Skovgaard, Drying technologies in food processing, Int. J. Food Microbiol. 129 (2009) 209. doi:10.1016/j.ijfoodmicro.2008.12.004.

[75] R. Feistel, W. Wagner, Sublimation pressure and sublimation enthalpy of H2O ice Ih between 0 and 273.16K, Geochim. Cosmochim. Acta. 71 (2007) 36–45. doi:10.1016/j.gca.2006.08.034.

[76] F.J. Rubio-Hernández, F. Carrique, E. Ruiz-Reina, The primary electroviscous effect in colloidal suspensions, Adv. Colloid Interface Sci. 107 (2004) 51–60. doi:10.1016/j.cis.2003.09.001.